Supporting Information

Tonicity-induced Cargo Loading into Extracellular Vesicles

Chaeeun Lee[a,b†], Sumit Kumar[a,b†], Juhee Park[b], Yongjun Choi[b], Elizabeth Maria[a,b], and Yoon-Kyoung Cho[a,b*]

[a]Department of Biomedical Engineering, Ulsan National Institute of Science and Technology (UNIST), Ulsan 44919, Korea.

[b]Center for Soft and Living Matter, Institute for Basic Science (IBS), Ulsan 44919, Korea.

†These authors contributed equally to this work.

* E-mail: ykcho@unist.ac.kr

Supplementary Discussion

Estimation of cargo loading into EVs by hypo-osmotic shock

To understand the cargo loading mechanism by hypo-osmotic shock, we employed the Kedem-Katchalsky (K-K) formalism. The model system is illustrated in **Figure S1** and the following two equations derived from the K-K formalism are utilized to calculate the relative volume increment and cargo concentration inside EVs.[1, 2]

$$\frac{dV_{rel}}{dt} = P_w V_w \frac{A}{V_0}\left(\frac{C_i^N + C_i^S(t)}{V_{rel}} - C_o^N - C_o^S\right) \quad (1)$$

$$\frac{dC_i^S(t)}{dt} = -P_s \frac{A}{V_0}\left(\frac{C_i^S(t)}{V_{rel}} - C_o^S\right) \quad (2)$$

Where P_w, P_S, V_w, V_0, and A are water permeability across the membrane, the permeability of cargo across the membrane, molar volume of water, initial EV volume, and surface area of vesicle, respectively. C_o^N and C_i^N are external and internal concentrations of nonpermeating solutes, respectively. C_o^S and C_i^S are external and internal concentrations of permeating solutes, respectively.

The simplified model, represented by equations 1 and 2, is based on the following key assumptions. These include a constant concentration in the external solution, consideration of only the concentration gradient across the EV membrane due to slower diffusion across the membrane, constant membrane thickness, and the direct proportionality of osmotic pressure to the concentration of the given substance.

The average EV radius, measured at 65.3 nm using DLS, served as the basis for the calculation of V_0 and A. Utilizing literature values for water permeability (Pw)[1, 2] at 5.8×10^{-5} m/s and Dox

permeability (PS)[3] at 5.0×10^{-7} m/s across cell membranes and the list of parameters shown in **Table S1**, the vesicle volume and Dox concentration inside EV as a function of time were calculated as shown in **Figure S2**.

Increasing Pw led to a rapid vesicle volume and cargo concentration escalation, as illustrated in **Figure S2A**. Variations in vesicle size influenced cargo loading dynamics, with larger vesicles requiring more time, as depicted in **Figure S2B**. The permeability of Dox, P_S, range from 0.1 to 25 μm/sec according to previous reports.[3, 4] The changes in Ps showed minimal effects on volume and cargo concentration within vesicles, as demonstrated in **Figure S2C**. The osmolarity of a hypotonic solution significantly impacted both volume increase and cargo concentration. However, when the osmolarity of the hypotonic solution fell below 296 μOsm/L, a plateau effect was observed, as shown in **Figure S2D**.

Based on the calculation using the conditions specified in **Table S1**, the theoretical cargo concentration inside the vesicle after 5 minutes is estimated to be 0.45 mM. This theoretical value may differ from the experimental result of 18.8 mM, derived by analyzing the Dox concentration in solutions collected from the top of the filter (representing total Dox concentration) and the flow-through samples (representing Dox concentration outside EVs). Several factors contribute to this variance. In the K-K equation, the concentration outside EVs is assumed to be constant over time. However, in real systems, osmolarity changes dynamically during filtration, creating a continual osmolarity difference between the interior and exterior of EVs. Additionally, the simulation assumes constant values for P_W and P_S, yet it is known that membrane permeability changes as vesicles undergo swelling.[5-7] This disparity between the assumptions of the simulation and the dynamic nature of the real system could be a contributing

factor to the observed differences in results.

Table S1. Parameters used in equation (1) and (2)

Parameters			References
P_w	5.80×10^{5}	m/s	[1]
V_w	18	cm^3/mol	[2]
A	5.35×10^{4}	nm^2	
V_0	1.16×10^{6}	nm^3	
r	65.3	nm	
P_S of Dox	5×10^{-7}	m/s	[3]
C_o^S	5×10^{-6}	M	
C_i^N	296	mOsm/L	
C_o^N	0.296	mOsm/L	

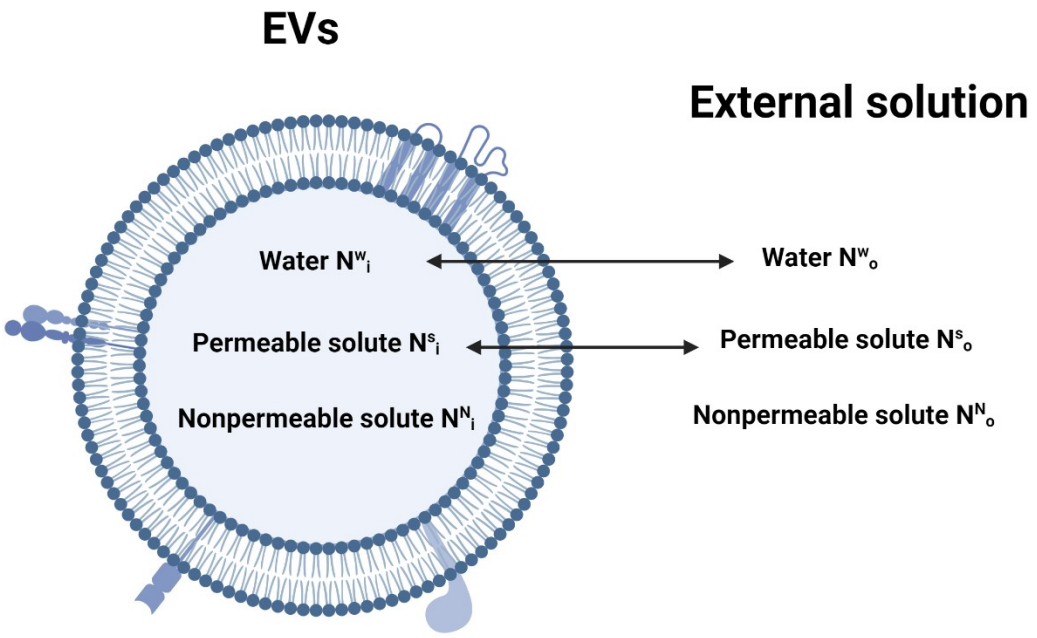

62

63 **Figure S1. Schematic representation of EVs under osmotic shock.** External solution contain

64 water (W), permeating solute (S), and non-permeating solute (N). Created by Biorender.

65

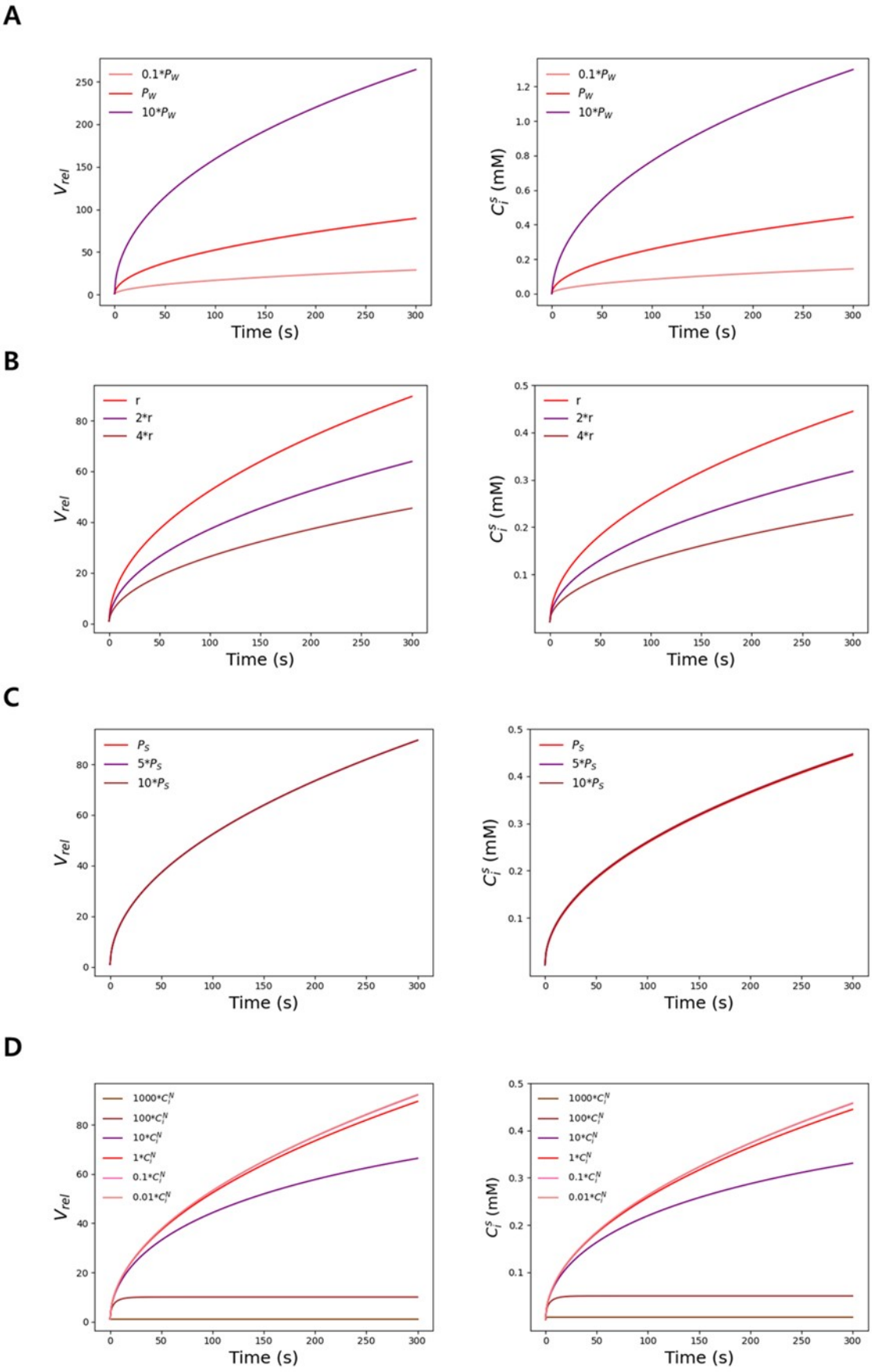
A
0.1*P_W
P_W
10*P_W
V_{rel}
Time (s)
C_i^s (mM)
B
r
2*r
4*r
C
P_S
5*P_S
10*P_S
D
1000*C_i^N
100*C_i^N
10*C_i^N
1*C_i^N
0.1*C_i^N
0.01*C_i^N

Figure S2. Simulation outcomes depicting the relative volume increment (left) and cargo concentration within EVs (right) over time with varied (A) water permeability across the membrane (P_w = 5.8×10^5 m/s), (B) radius of vesicle (r = 65.3 nm), (C) permeability of cargo across the membrane (P_S = 5.0×10^{-7} m/s), (D) the osmolarity of hypotonic solution outside EVs (C_o^N = 0.296 mOsm/L). The parameters are summarized in **Table S1**.

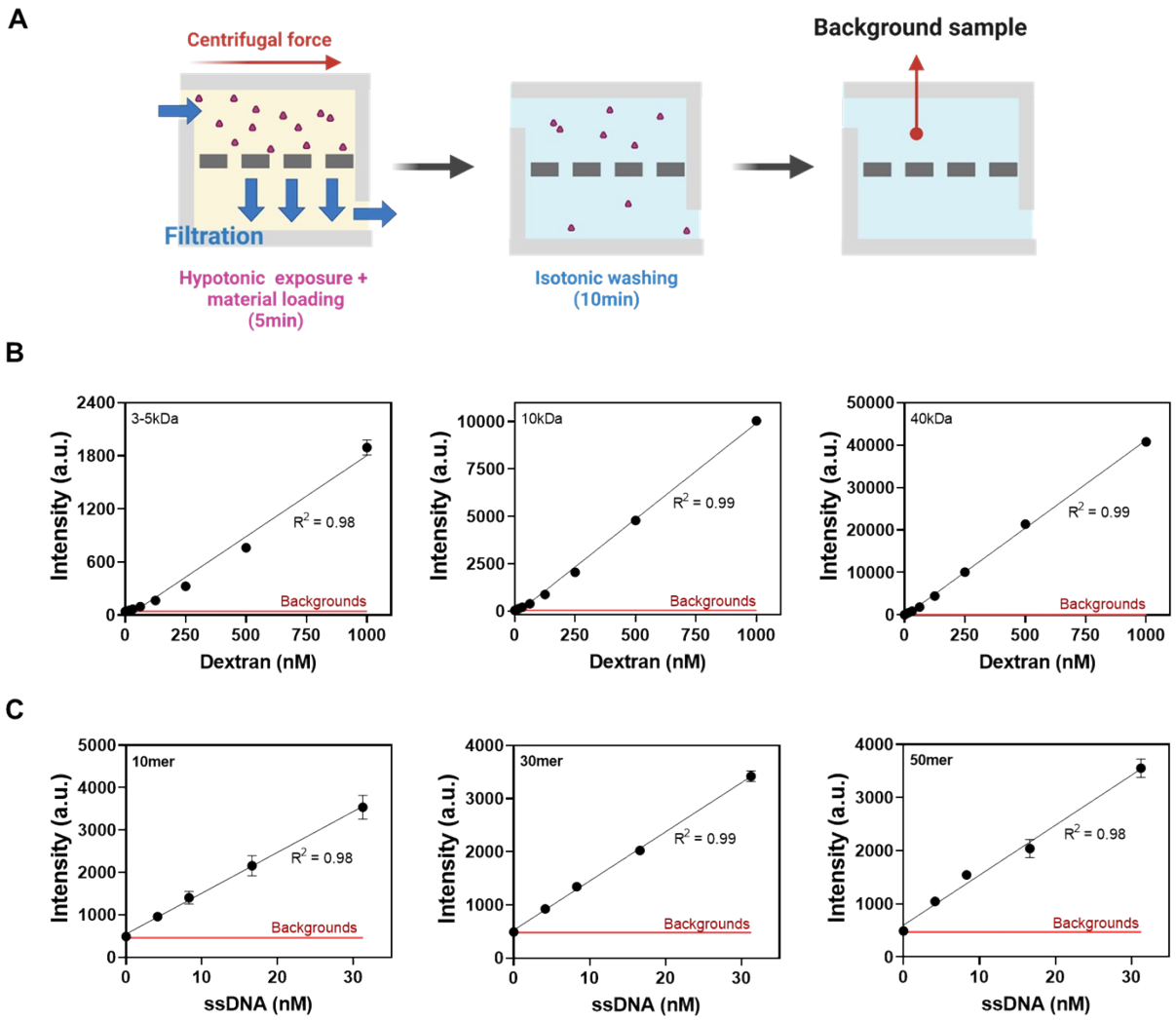

Figure S3. To confirm the effective washing of free loading materials, the background signal is compared with the calibration curve. (A) Illustration of the preparation process of the background sample. (B) Background signals of (i) 3-5 kDa, (ii) 10 kDa, and (iii) 40 kDa FITC-dextran respectively, along with their corresponding calibration curves. (C) Background signals of (i) 10 mer, (ii) 30 mer, and (iii) 50 mer FAM labelled ssDNA respectively, along with their corresponding calibration curves. Each point represents a triple replication, and in some cases, the error bars are too small to be seen.

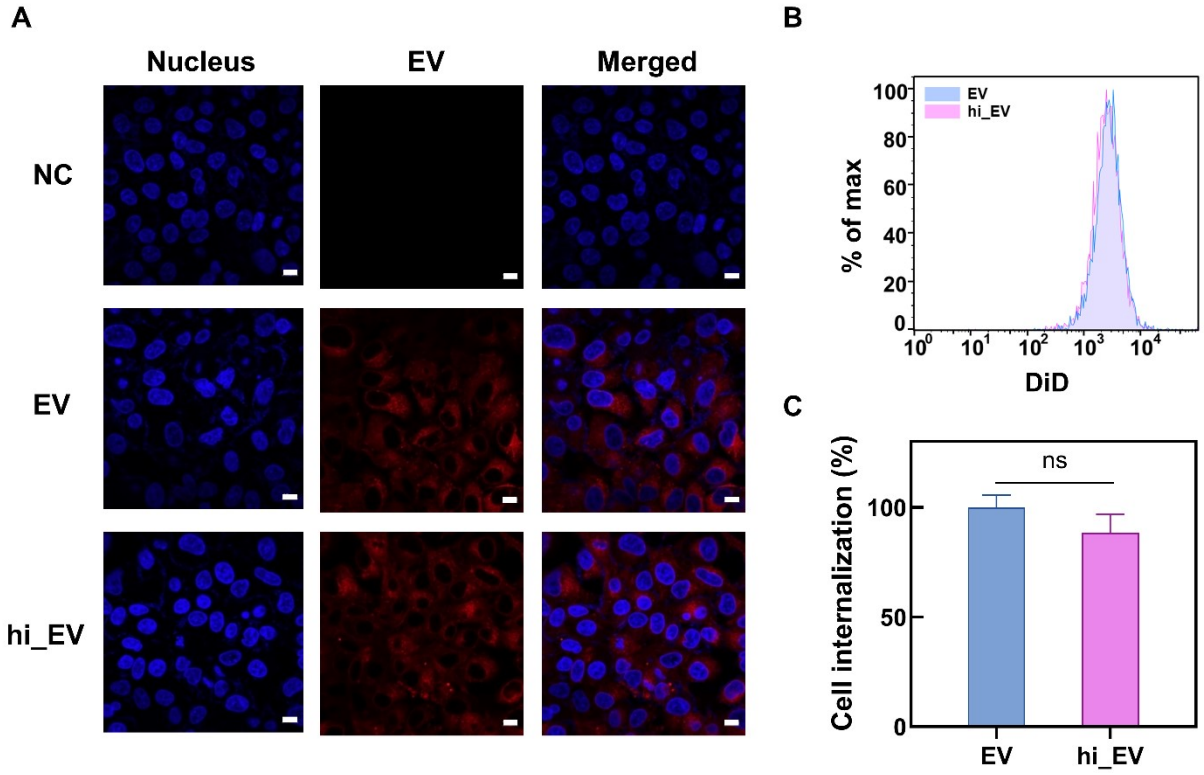

Figure S4. TC method does not impair the cellular internalization of EVs (A) Confocal microscopy images of the internalization of HEK293T EVs stained with DiD (red) into A549 cells, with the cell nucleus stained with Hoechst 33342 (blue) (NC; negative control, scale bar: 10 μm). (B) Fluorescence-activated cell sorting (FACS) analysis represents the EV-treated cells' fluorescence intensity. (C) The efficiency of EV internalization into cells was calculated using the mean fluorescence intensity (MFI) determined by FACS (ns, not significant; *p > 0.05). Data represent mean ± s.d. of *n* = 3 independent experiments.

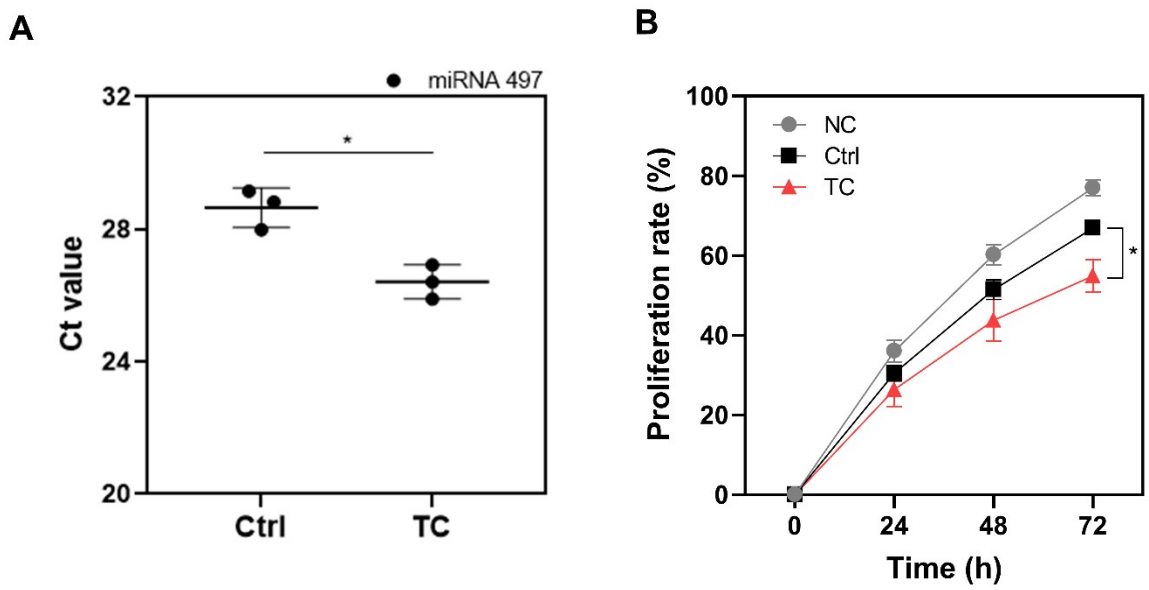

Figure S5 Quantification results of the loading of miR-497 into EVs using the TC method, and the results of proliferation test performed on A549 cells after treatment of miR-497 loaded EVs. (A) The Ct value measured by real-time PCR after loading miR-497 into EVs using the TC method is compared with the control case (*$p < 0.05$). (B) Proliferation rate is measured after treating A549 cells with miR-497 loaded EVs (*$p < 0.05$). The data represent the mean ± s.d. of $n = 3$ independent experiments.

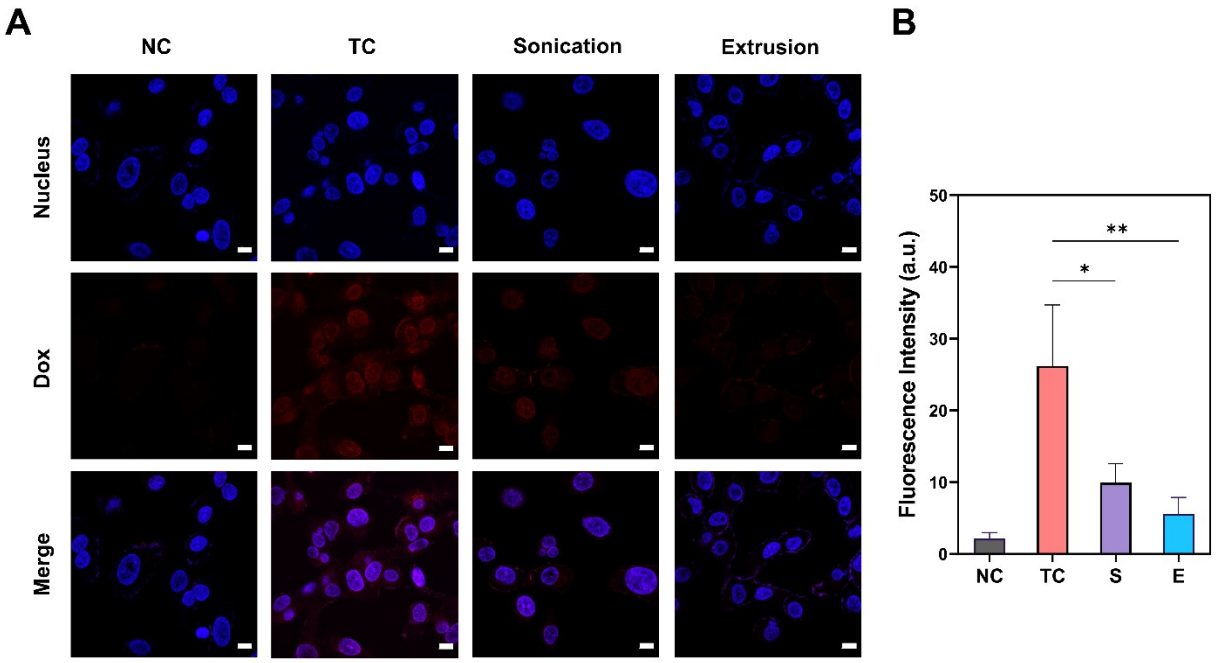

Figure S6. Analysis of Dox-EV internalization in A549 cells depending on the loading methods (A) Representative images of A549 cells after treating with Dox-EVs. (Nucleus is stained blue and Dox-EV is stained red, scale bar: 10 μm) (B) Quantification of the mean fluorescence intensity (MFI) of Dox. Data shown as mean ± s.d. of n = 3 independent experiments (** $p < 0.01$, * $p < 0.05$).

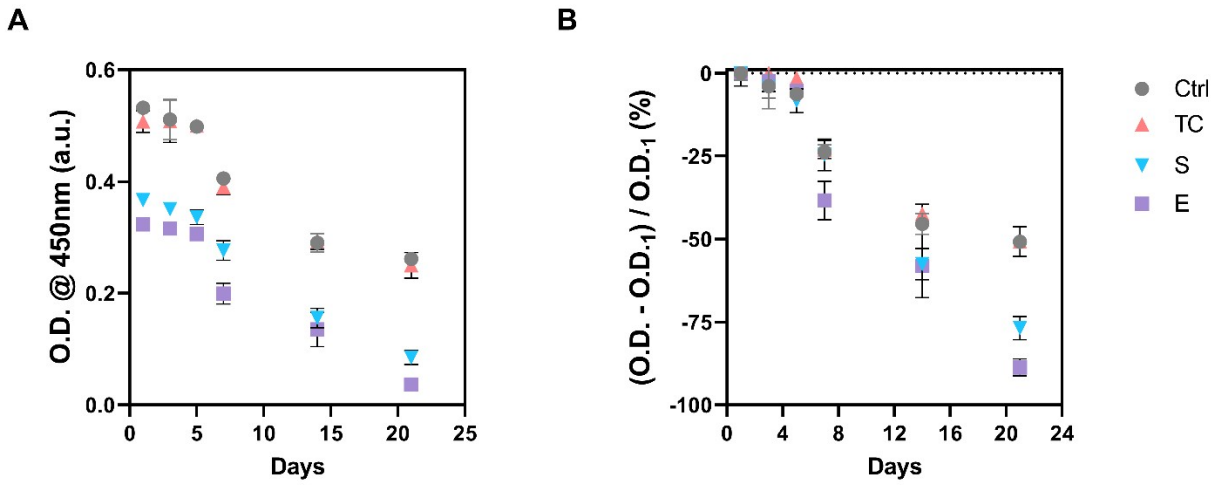

Figure S7. Stability assessment of EVs after different loading procedures. The stability of EVs was evaluated using sandwich ELISA employing tetraspanin markers (CD81 as capture antibody and CD9 as detection antibody). (A) EV stability was observed after distinct loading methods: TC (tonicity control), S (sonication), and E (extrusion). (B) Percent decrease in signal normalized to their day 1 values (O.D. ; optical density, O.D.1; optical density at day1) after each process. After 21 days of storage at 4°C, Ctrl and TC samples exhibited a signal decrease of 51.0 ± 1.7% and 53.0 ± 4.3%, respectively, compared to day 1. Sonication and extrusion showed a more pronounced signal reduction of 76.9 ± 3.5% and 88.7 ± 2.6%, respectively.

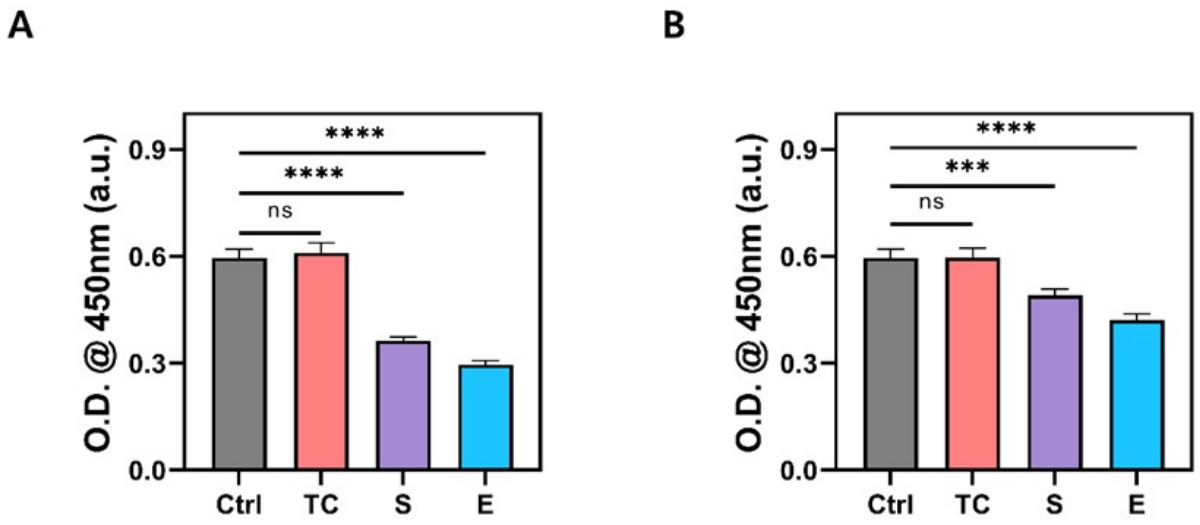

Figure S8. Comparison of TC with other EV loading methods by using sandwich ELISA (capture antibody: CD81 and detection antibody: CD9) (TC, tonicity control; S, sonication; E, extrusion) (A) CD81-CD9 ELISA results after each process when the same initial CCS volume was used. (B) CD81-CD9 ELISA results using EV samples with the same particle concentration after various loading processes. (****$p < 0.0001$; ***$p < 0.001$; ns, not significant)

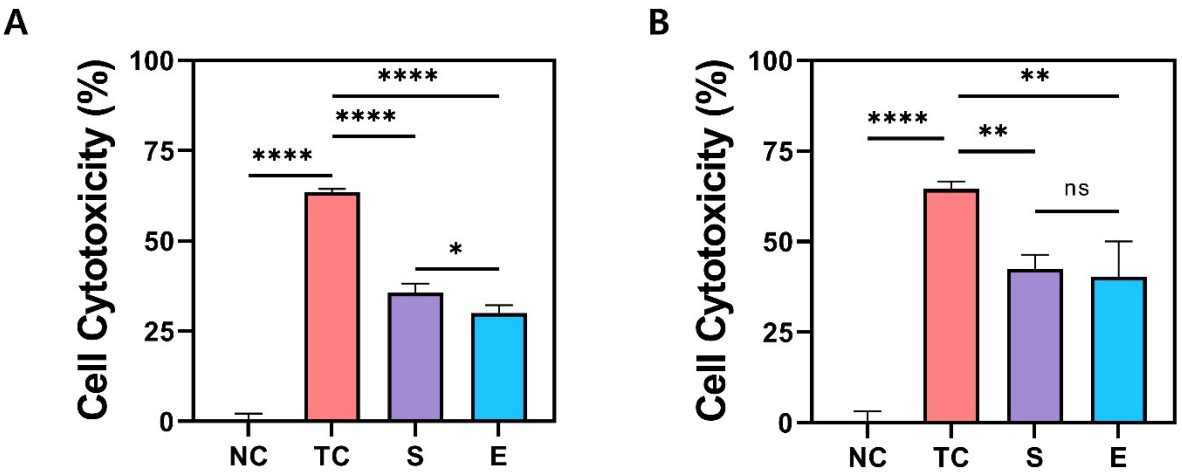

Figure S9. A549 cell cytotoxicity after 48 hrs by treating Dox-EVs produced by different processes (A) Cell cytotoxicity after treating Dox-EVs obtained from the experiments using the same initial volume of CCS. (B) Cell cytotoxicity after treating with equal particle concentrations of EVs obtained from different loading processes. (****p < 0.0001, **p < 0.01; ns, not significant).

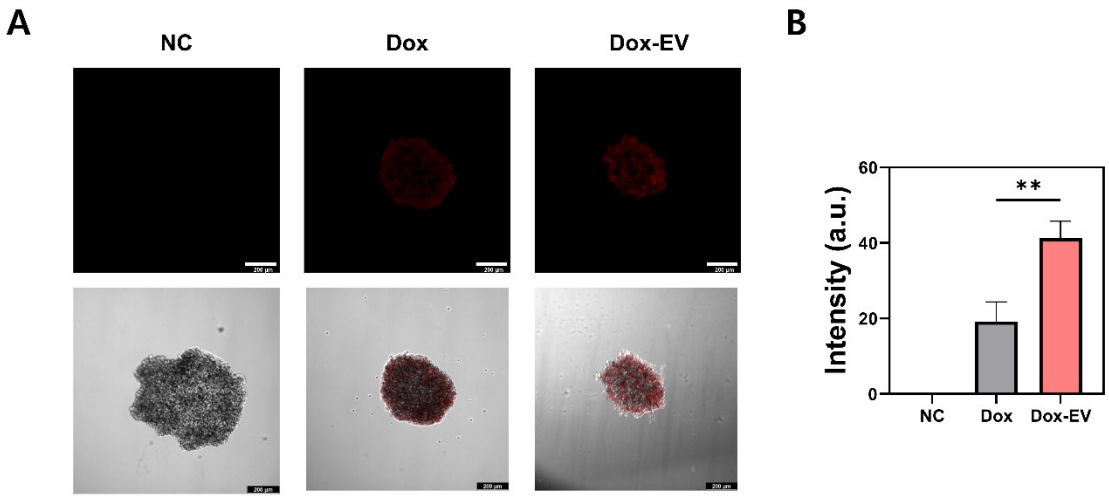

Figure S10. Confocal imaging of A549 spheroids treated with Dox and Dox-EV produced by TC methods (Scale bar = 200 µm) Images were captured using a confocal microscope (THUNDER, Leica) at 10X magnification. Dox-EV intensity within the spheroids was evaluated by generating images using max intensity projection of Z-stack via the THUNDER imaging system. (A) Cellular uptake and distribution of Dox and Dox-EVs after the treatment for 48 hrs. (B) Mean intensity of Dox inside of the spheroid area. (**$p < 0.01$)

References

1. J. R. W. a. M. Elimelech*, *Science Advances*, 2018, **4**, eaar8266.
2. H. Y. Elmoazzen, J. A. Elliott and L. E. McGann, *Biophys J*, 2009, **96**, 2559-2571.
3. G. Speelmans, R. W. Staffhorst, B. de Kruijff and F. A. de Wolf, *Biochemistry*, 1994, **33**, 13761-13768.
4. Z. Aminipour, M. Khorshid, H. Keshvari, S. Bonakdar, P. Wagner and B. Van der Bruggen, *Eur J Pharm Biopharm*, 2020, **146**, 133-142.
5. S. U. Alam Shibly, C. Ghatak, M. A. Sayem Karal, M. Moniruzzaman and M. Yamazaki, *Biophys J*, 2016, **111**, 2190-2201.
6. D. Kumar, A. Gayen and M. Chandra, *ACS Infect Dis*, 2023, **9**, 2471-2481.
7. C.-M. Lin, D. T. Wu, H.-K. Tsao and Y.-J. Sheng, *Soft Matter*, 2012, **8**.